

H₂O Masers in W 49 North and Sagittarius B 2

Elizabeth J.M McGrath¹

Institute for Astronomy, University of Hawaii, Honolulu, HI 96822

mcgrath@ifa.hawaii.edu

W .M .G oss

National Radio Astronomy Observatory, Socorro, NM 87801

mgoss@nrao.edu

and

Christopher G .D eP ree

D epartment of Physics and A stronomy, Agnes Scott College, Decatur, GA 30030

cdepree@agnesscott.edu

A B S T R A C T

Using the Very Large Array (VLA) of the National Radio Astronomy Observatory in the A and B configurations, we have obtained simultaneous high resolution observations of both the 22 GHz H₂O maser lines as well as the 22 GHz continuum for the H ii regions W 49N and Sagittarius B 2. The angular resolution of both observations is 0⁰.1, which at the distance of W 49N (11.4 kpc; Winn, Moran, & Reid 1992) and Sgr B 2 (8.5 kpc) corresponds to a physical size of < 1000 AU in both sources. The velocity coverage for W 49N is 435 km s⁻¹; positions for 316 H₂O maser components were obtained. The velocity coverage for Sgr B 2 is -40 to +120 km s⁻¹; positions for 68 maser components were determined in Sgr B 2 Main, 79 in Sgr B 2 North, 14 in Sgr B 2 Mid-North, and 17 in Sgr B 2 South, for a total of 178 H₂O maser positions in Sgr B 2.

The cross calibration scheme of Reid & Menten (1990, 1997) was used. Using this procedure, high dynamic range continuum images were obtained with accurate registration (~ 0⁰.01) of the continuum and maser positions. A detailed comparison between H ii components and maser positions for both Sgr B 2

¹NSF sponsored REU student, National Radio Astronomy Observatory

and W 49N is presented. In Sgr B2 Main, the H₂O masers are predominantly located at the outside edge of the high-frequency continuum, lending support to the proposal that entrainment by stellar winds may play an important role in H₂O maser emission.

Subject headings: H ii regions | ISM : individual (Sagittarius B2, W 49A) | masers

1. Introduction

H₂O masers have long been known to be signposts of active star formation and regions of extremely dense ($> 10^6 \text{ cm}^{-3}$) gas. As such, they have proven to be very useful tools to study the dynamics and kinematics of the environment around young, massive stars, tracing high velocity outflows and shock fronts (Elitzur 1995). Additionally, masers are extremely short-lived phenomena, and therefore pinpoint a precise period in a star's evolution. In particular, H₂O masers are often associated with ultra-compact (UC) H ii regions, the short-lived phase that can be associated with massive stars as they move towards the main sequence and produce UV photons which ionize the nearby gas (eg., Garay & Lizano 1999).

These observations focus on two well-known high mass star forming regions in our galaxy, W 49A and Sgr B2. W 49A has been studied extensively at radio wavelengths (eg., Mezger, Schraml, & Terzian 1967; Moran et al. 1973; Walker, Matsuakis, & Garcia-Barreto 1982; Winn, Moran & Reid, 1992; DePree et al., 2000). Mezger et al. (1967) observed W 49A to have two thermal components: A2, a small (diameter = 1 pc) high-density ($n_e = 10^4 \text{ cm}^{-3}$) source embedded in a second source, A1, which is larger (diameter = 14 pc) and lower density ($n_e = 200 \text{ cm}^{-3}$). In their investigation, Mezger et al. (1967) pointed out that the high-density sources might surround O stars still embedded in their ionized dust cocoons. W 49A has also been the subject of several investigations at infrared (IR) wavelengths. Conti & Blum (2002) have carried out near-infrared observations of the W 49A region that indicate the presence of approximately 100 O stars. Alves & Homeier (2003) have also observed this region in the near-IR, and their J, H, and K band images indicate the presence of four star-forming clusters in W 49A.

Located within W 49A, the source W 49N is composed of several compact and ultra-compact H ii regions in a ring formation spanning $20''$, or 1pc in diameter (e.g., DePree et al. 2000). Fig. 1 shows the 3.6 cm continuum image of the entire W 49A complex with the H ii regions where maser activity is prominent (W 49N) indicated. These regions are shown in more detail in the inset 1.3 cm images. The H ii region G 1/G 2 is the main locus of water masers in W 49N, along with a smaller cluster of H₂O masers located near the

H ii region B1/B2. The H₂O maser velocity distribution in W 49N is known to span at least 560 km s⁻¹ (Walker et al. 1982), and is the most luminous source of H₂O maser activity in the Galaxy.

The Sgr B2 star-forming region and its ultra- and hyper-com pact H ii regions have also been studied in great detail (eg., Gauvin et al. 1995; Depree et al. 1995, 1996; Depree, Goss & Gauvin 1998). A variety of morphologies are found among the H ii regions, including ring, shell, arc, and cometary structures. The entire Sgr B2 complex covers an area of 1° 2°, or 2.5–5 pc (see Fig. 2), which consists of more than 49 H ii regions, 3 of which exhibit maser activity, and a fourth region that shows maser activity but no associated H ii region (Kobayashi et al. 1989). The K2 region in Sgr B2 North (Fig. 2b) is a region of strong H₂O maser activity and is coincident with the dynamical center of molecular outflow (Lis et al. 1993). Depree et al. (1995) suggest that this source is similar to source F in Sgr B2 Main (Fig. 3), another region of intense H₂O maser emission and bipolar molecular outflow (Lis et al. 1993; Mahringer, Goss, & Palmer 1995a). Additionally, age determinations suggest that the Sgr B2 Main complex of H ii regions and the molecular outflow are related (Depree et al. 1996). From observations of H110 and H₂CO towards Sgr B2 North and Main, Mahringer et al. (1993, 1995b) find that Sgr B2 North is probably more distant, and suggest that two or more different events triggered star formation in each core, rather than a single global star formation event. Takagi et al. (2002) find strong X-ray sources located in Sgr B2 Main associated with the H ii regions F3 and I, as well as a weaker source near Sgr B2 North. The X-ray spectra and luminosities are consistent with emission arising from groups of young stellar objects (YSOs).

The study of H₂O masers in high mass star-forming regions has provided an important contribution to both observation and theory relating to YSO molecular outflows. Studies of water masers in W 49 have been carried out with single dish antennas (Morris 1976) and Very Long Baseline Interferometry (VLBI) (Moran et al. 1973; Walker et al. 1982; Winn et al. 1992). Previous observations of water masers in Sgr B2 have been carried out with VLBI (Reid et al. 1988) and the Nobeyama Millimeter Array (Kobayashi et al. 1989). The resolution and subsequent absolute positions from Kobayashi et al. (1989) have rms errors of 1°.0–3°.0 (), while the relative positions have rms errors of 0°.3. In order to perform a detailed comparison between the UC H ii regions and the maser positions, sub-arcsec resolution and positional accuracy is required. The current observations provide an unprecedented velocity coverage of H₂O masers in both W 49N and Sgr B2, covering a range of 870 and 160 km s⁻¹ respectively, with angular resolutions of 0°.1. At the distance of W 49N (11.4 kpc; Winn et al. 1992), this resolution corresponds to a physical size of 0.005 pc, and for Sgr B2 at 8.5 kpc, this angular size corresponds to 0.004 pc, i.e. < 1000 AU in both cases. Additionally, the uncertainty of the relative positions of the H₂O masers

is 0.005, or a factor of at least ten better than previous observations of W 49 (Gwinn et al. 1992), and 100 times improved over previous data for Sgr B2 (Kobayashi et al. 1989). With the increased precision and velocity coverage of the current data, we can for the first time accurately compare the positions of H₂O masers and the UC H ii regions in these two sources, as well as gain a better understanding of the environments near these young stellar objects.

2. Observations

Observations of W 49N and Sgr B2 were carried out with the VLA in both A and B configurations using the correlator in line mode with 2 IFs at 22 GHz. Tab. 1 summarizes the parameters of these observations. All maser observations had 63 channels per IF, with a bandwidth of 3.125 MHz, resulting in a velocity resolution of 0.66 km s⁻¹ and a total velocity coverage of 41.6 km s⁻¹ for each observation. In each case, IF1 was centered on velocity multiples of 30 km s⁻¹ from the H₂O 6₁₆ - 5₂₃ line transition at 22.23508 GHz, which provided some overlap between observations to allow for the decreased sensitivity at the band edges. The velocity of 170 km s⁻¹ was chosen as the central velocity of IF2 for both sources. In W 49N, this velocity corresponds to a bright maser feature which was used both as a positional reference point and to self-calibrate the data (see x2.1). In Sgr B2, this velocity is line free, which allowed us to obtain continuum images simultaneously with the line observations. Integration times were approximately 15 minutes for each of the 29 velocity cubes in W 49N, for a total of 7.3 hours on W 49N, and 20 minutes for each of the 5 velocity cubes in Sgr B2, for a total of 1.7 hours on Sgr B2. The primary phase calibrators for W 49N and Sgr B2 were 1932+210 (1.44 Jy) and 1730-130 (4.73 Jy), respectively, and the primary flux density calibrator was 3C 286.

2.1. W 49

For W 49N, we were able to self-calibrate the line cube data using a strong maser feature ($S > 50$ Jy) at 170.7 km s⁻¹ in IF2, observed in parallel during all observations. After self-calibration the typical rms noise values were 1.0 Jy beam⁻¹ in a line-free channel, and 0.25 Jy beam⁻¹ in channels with a 10-50 Jy beam⁻¹ H₂O maser feature. For the W 49N 1.3cm August 1998 continuum data, IF1 was centered on $v = 500$ km s⁻¹. At this velocity, there are no detectable H₂O masers. We were then able to use the strong maser feature at 170.7 km s⁻¹ in IF2 to cross-calibrate the broad-band continuum at $v = 500$ km s⁻¹ in IF1 using the technique outlined by Reid & Menten (1990, 1997). This technique utilizes

the phase and amplitude corrections obtained from self-calibrating the maser emission at $v = 170.7 \text{ km s}^{-1}$ in IF2, applying these corrections to the broad-band continuum in IF1. The resulting rms noise in the continuum was $4.3 \text{ mJy beam}^{-1}$. Further details of the reduction of the 1.3 cm continuum data are presented by DePree et al. (2000).

In order to obtain an improved alignment between the H_2O masers and the 1.3 cm continuum, we assumed that the position of the 170.7 km s^{-1} maser feature in IF2 as observed with the August 1998 continuum data was fixed. Then all other observations of the 170.7 km s^{-1} maser were shifted by small amounts (typically < 0.05 in both α and δ) in order to align the various epochs. The shifts required to bring the IF2 170.7 km s^{-1} maser features into agreement with the position of the reference maser at 170.7 km s^{-1} in the August 1998 data were then applied to the IF1 maser line cubes using the AIPS task OGEOM. This method assumes negligible proper motion of the reference maser feature over the length of the observations (1 year). In the case of W 49N, this procedure is justified since typical proper motions of these masers are on the order of a few mas per year (Gwin et al. 1992). This calibration technique allowed us to obtain a relative maser alignment with respect to the 1.3 cm continuum of 0.01 , and a relative positional accuracy of 0.005 between the masers.

2.2. Sgr B 2

For Sgr B 2, the maser lines and the continuum were observed simultaneously in order to cross-calibrate the continuum with the masers, again following the technique of Reid & Menten (1990, 1997). The line data was first self-calibrated, and then the corrections were applied to the line-free continuum in IF2. Each line cube was therefore accurately aligned to its corresponding continuum. The typical rms noise obtained for the Sgr B 2 observations was similar to that of W 49 (1.0 Jy beam^{-1} in a line-free channel).

The centroids of the H ii regions in the continuum observed with the IF1 velocity cube at 40 km s^{-1} were found to agree with positions tabulated in Gaume et al. (1995) to within their quoted rms errors of 0.01 in α and 0.1 in δ . This continuum was used as a reference for the other data cubes. We then shifted each observation in order to match this continuum, and applied these shifts to each corresponding IF1 line cube. Once again, shifts were typically < 0.05 in α and δ . The rms error in the alignment of the H_2O masers and the continuum was again 0.01 , with a relative positioning accuracy of 0.005 for the maser features in Sgr B 2.

3. Results

3.1. W 49

Over the velocity range -435 km s^{-1} to $+435 \text{ km s}^{-1}$, we find 316 H_2O maser components between velocities -352.1 and 375.5 km s^{-1} in W 49N. The positions, velocities and flux densities of these H_2O masers are listed in Tab. 2 and a spectrum of the masers is shown in Fig. 4. The same three regions of prominent maser activity noted by Moran et al. (1973), Walker et al. (1982), and Winn et al. (1992) around H ii regions G 1/G 2 are observed, as well as the separation between blueshifted features to the west and redshifted features to the east of the outflow center (see Fig 1). The high and low velocity features co-exist in the region around the center of outflow, while at greater distances from the outflow center, only high velocity features are observed. In addition to the masers surrounding the UC H ii regions G 1 and G 2, there is another cluster of masers to the west around H ii region B 2 (see Fig 1). This cluster consists mostly of OH masers (from Argon, Reid, & Menten 2000), but a few redshifted H_2O masers (100 km s^{-1}) are detected there as well, which suggests that these H_2O masers are not associated with the G 1/G 2 outflow, since all other H_2O masers west of source G 1 are blueshifted. Approximately 16° to the northeast of source G 2 there is a cluster of H_2O masers that is not associated with any prominent H ii region. The velocity range of these masers is from 5.3 km s^{-1} to 121.3 km s^{-1} . There is also a group of OH masers at the 1612 MHz transition (Argon et al. 2000) approximately $3^{\circ}5$ north of source A, that are not associated with any detected H ii region.

3.2. Sgr B 2

In Sgr B 2, a velocity range of -40 km s^{-1} to 120 km s^{-1} was investigated. We detected 79 H_2O masers in Sgr B 2 North between -16.1 and 119.8 km s^{-1} (Fig. 2b), 14 masers in Sgr B 2 Mid-North between 23.8 and 117.8 km s^{-1} (Fig. 2c), and 17 masers in Sgr B 2 South between 3.4 and 82.8 km s^{-1} (Fig. 2d). In Sgr B 2 Main we detected 68 masers between -13.4 and 117.1 km s^{-1} which are plotted over the high resolution 7mm continuum image of Depree et al. (1998) in Fig. 3 along with the OH masers detected by Argon et al. (2000). Absolute positional errors for the OH masers are 0.3 arcseconds, while the absolute alignment between the H_2O masers and the 7mm continuum is 0.05 . Figures 5 and 6 show the entire spectrum of maser emission in Sgr B 2 Main and North, and Mid-North and South, respectively, while Tables 3 – 6 list the positions, velocities, and flux densities of the H_2O masers detected in all Sgr B 2 regions.

In Sgr B 2 North, the H_2O maser positions center around K 2 (see Fig. 2b), while the OH

masers are clustered around K 3. The H₂O masers in Sgr B2 Mid-North shown in Fig. 2c are coincident with the OH masers around the compact source labeled Z10.24 by Gaume et al. (1995). A few (< 10) high and low velocity H₂O masers are visible to the west, which may indicate another region of outflow. In Sgr B2 South, the H₂O and OH masers are coincident around the front edge of the cometary source H, and have comparable velocities. A clump of mostly low velocity H₂O masers to the west of source H is detected. Another clump of OH masers is detected between source H and the outlying H₂O masers to the west.

4. Discussion

4.1. W 49

The observed H₂O maser velocity range (-352 to 375 km s⁻¹) is the largest observed for any region in the Galaxy to date, making W 49N a truly exceptional H₂O maser source. Due to prominent time variations in the maser emission (e.g., Sullivan 1971), however, observations at other epochs may well exhibit a different velocity extreme. Morris (1976) suggests a smaller velocity range for W 49N (-256 to +271 km s⁻¹), albeit still large by comparison to other active H₂O maser regions in the Galaxy. Gwinn et al. (1992) suggest that the H₂O masers in W 49N are accelerating from a common origin in a bipolar outflow. The high resolution continuum imaging of DePree et al. (2000) indicates that the center of this high velocity outflow lies directly between the two ultra-compact H II regions, G 1 and G 2a.

The majority of the OH masers detected by Argon et al. (2000) appear to be clustered around source B2, where there is limited H₂O maser emission. Additionally, Gaume & Mutil (1987) find a larger cluster of OH masers around the main region of H₂O maser activity, sources G 1 and G 2. The relative strength of OH and H₂O masers in these two H II regions may indicate different evolutionary stages, or simply different excitation levels due to the number of stars producing UV radiation in each region. Water masers are typically associated with the presence of young O and B stars, but are also found to be associated with even younger sources like hot molecular cores, and in these cases are thought to trace the outflows associated with young stellar objects (e.g. DeBuizer et al. 2000). Some examples of possible hot cores indicated by the H₂O maser data include the region 16° to the northeast of sources G 1/G 2 and the group of OH masers 3°.5 north of source A, where maser activity is observed but no associated H II region is detected. Wilner et al. (2001) find CH₃CN emission at the former position which they attribute to a hot core, but do not detect any CH₃CN emission at the latter location.

4.2. Sgr B 2

From Fig. 3, we can see that the H₂O maser positions in Sgr B 2 Main fall almost perfectly along the outside edge of the 7mm continuum. One interpretation of this alignment, is that entrainment may play a role in maser formation, whereby the masers form in the dense material swept up by the stellar winds. Alternatively, these masers may be associated with the molecular outflow of the Sgr B 2 F region itself (e.g. Kuan & Snyder 1996). OH masers in Sgr B 2 Main are detected farther from the 7mm continuum, and there appears to be a dichotomy between the H₂O and OH masers; the H₂O masers are found primarily around source F1, whereas the majority of OH masers are found to the south of F3. Torrelles et al. (1997) find a similar dichotomy in the relative positions of OH and H₂O masers in W 75N; the H₂O masers appear to be aligned more closely along the outflow axis, while the OH masers appear to be more distant. They note that this arrangement is consistent with the idea proposed by Forster & Caswell (1989) in which OH masers are formed at a later stage in the lifetime of the YSO, in the less dense surrounding material, but they also examine the possibility that the OH masers trace an older outflow region, distinct from that of the H₂O masers.

In Sgr B 2 North we see another dichotomy between H₂O and OH masers. The velocities of the OH masers are lower than the velocities of the H₂O masers at the same position, so it is possible that as suggested for Sgr B 2 Main, the H₂O and OH masers may trace different outflows, or the OH masers may trace an older outflow event. A few clusters of masers were discovered in areas not associated with an H II region, notably the area west of Z10.24 in Sgr B 2 Main North, and two regions west of source H in Sgr B 2 South. Each of these may indicate hot cores in various evolutionary stages and of various intensities, given the differences in the relative contribution from both H₂O and OH masers at each location.

5. Conclusions

Positions and velocities for 316 and 178 1.3cm H₂O maser components have been determined in the massive H II regions, W 49N and Sgr B 2, respectively. These represent the best velocity coverage and relative maser positions to date for these sources. The relative positions of the continuum and maser positions have been determined to a level of 0.01, while the relative positions of the H₂O maser components have a precision of 0.005. Both sources show high velocity outflows and strong maser emission regions, indicative of active star formation.

W 49N and Sgr B 2 show similarities in the velocity structure of masers around a center

of outflow; close to the center, a range of maser velocities is observed, while farther away only high velocity features are present. This type of structure can be explained with the model proposed by Mac Low & Blitz (1992), where the maser features lie along a shocked shell expanding outwards from a central star or group of stars, driven by a strong central wind. Alternatively, Winn et al. (1992) suggest that the masers trace the bipolar outflow itself and that a shell of shocked emission is not a necessary condition for maser formation.

Additionally, we find that the OH and H₂O masers in W 49N and SgrB2 appear to trace different regions, which could be interpreted as an evolutionary effect; the younger sources predominantly give rise to H₂O masers, while the older outflows excite OH masers. In both W 49N and SgrB2, the H₂O masers are found in denser regions (as traced by molecular gas) than the OH masers, tracing out the very edge of the 7mm continuum. These observations support the idea that clumps of dense gas from which the H₂O masers originate may be entrained by stellar winds sweeping up the gas into an expanding shell.

Finally, several regions of H₂O maser activity have been detected that do not appear to correspond with H II regions (far northeast of source G in W 49N, north of source A in W 49N, west of source Z1024 in SgrB2 Mid-North, and two regions west of source H in SgrB2 South). These represent regions for further study, as they may pinpoint stars in the earliest stages of formation, surrounded by hot cores still moving onto the main sequence.

The authors wish to thank Crystal Brogan and the anonymous referee for helpful comments on the text, as well as Mark Reid for his advice during the initial stages of the project. EJM greatly acknowledges support from the NSF funded Research Experience for Undergraduates Program, which helped fund a part of this research. EJM also thanks the Brandeis radio astronomy group for their hospitality at Brandeis University, where some of the data reduction was completed. The National Radio Astronomy Observatory is a facility of the National Science Foundation operated under cooperative agreement by Associated Universities, Inc.

R E F E R E N C E S

- A lves, J., & H o m e i e r, N . 2003, ApJ, 589, L45
- A rgon, A . L ., R eid, M . J ., & M enten, K . M . 2000, ApJS, 129, 159
- C ont i, P . S ., & B lum , R . D . 2002, ApJ, 564, 827
- D e B uizer, J. M ., P ina, R . K ., & T elesco, C . M . 2000, ApJS, 130, 437
- D eP ree, C . G ., G aum e, R . A ., G oss, W . M ., & C laussen, M . J . 1995, ApJ, 451, 284
- D eP ree, C . G ., G aum e, R . A ., G oss, W . M ., & C laussen, M . J . 1996, ApJ, 464, 788
- D eP ree, C . G ., M ehringer, D . M ., & G oss, W . M . 1997, ApJ, 482, 307
- D eP ree, C . G ., G oss, W . M ., & G aum e, R . A . 1998, ApJ, 500, 847
- D eP ree, C . G ., W iiner, D . J ., G oss, W . M ., W elch, W . J ., & M cG rath, E . J . 2000, ApJ, 540, 308
- E litzur, M . 1995, in RevM exAA Ser. de Conf. 1, C ircum stellar D isks, O ut ows and Star Formation, eds. S . Lizano, & J.M . Torrelles (Cozum el, M exico: RevM exAA), 85
- G aray, G ., & L izano, S . 1999, PA SP , 111, 1049
- G aum e, R . A ., C laussen, M . J ., D eP ree, C . G ., G oss, W . M ., & M ehringer, D . M . 1995, ApJ, 449, 663
- G aum e, R . A ., & M utel, R . L . 1987, ApJS, 65, 193
- G w inn, C . R ., M oran, J. M ., & R eid, M . J . 1992, ApJ, 393, 149
- F orster, J. R ., & C aswell, J. L . 1989, A & A , 213, 339
- K obayashi, H ., I shiguro, M ., C hikada, Y ., U kita, N ., M orita, K .-I ., O kum ura, S .K ., K asuga, T ., & K awabe, R . 1989, PA SJ , 41, 141
- K uan, Y .-J ., & S nyder, L . E . 1996, ApJ, 470, 981
- L is, D . C ., G oldsm ith, P . F ., C arlstrom , J. E ., & S coville, N . Z . 1993, ApJ, 402, 238
- M ac Low , M . M ., & E litzur, M . 1992, ApJ, 393, 33
- M ehringer, D . M ., P almer, P ., G oss, W . M ., & Yusef-Zadeh, F . 1993, ApJ, 412, 684

- Mehringer, D. M., Goss, W. M., & Palmer, P. 1995a, *ApJ*, 452, 304
- Mehringer, D. M., Palmer, P., & Goss, W. M. 1995b, *ApJS*, 97, 497
- Mezger, P. G., Schraml, J., & Terzian, Y. 1967, *ApJ*, 150, 807
- Moran, J. M., Papadopoulos, G. D., Burke, B. F., Lo, K. Y., Schwartz, P. R., & Thacker, D. L. 1973, *ApJ*, 185, 535
- Morris, M. 1976, *ApJ*, 210, 100
- Reid, M. J., & Menten, K. M. 1990, *ApJ*, 360, L51
- Reid, M. J., & Menten, K. M. 1997, *ApJ*, 476, 327
- Reid, M. J., Schneps, M. H., Moran, J. M., Winn, C. R., Genzel, R., Downes, D., & Ronnang, B. 1988, *ApJ*, 330, 809
- Sullivan, W. T., III 1971, *ApJ*, 166, 321
- Takagi, S., Murakami, H., & Koyama, K. 2002, *ApJ*, 573, 275
- Torrelles, J. M., Gomez, J. F., Rodriguez, L. F., Ho, P. T. P., Curiel, S., & Vazquez, R. 1997, *ApJ*, 489, 744
- Walker, R. C., Matzakis, D. N., & Garcia-Barreto, J. A. 1982, *ApJ*, 255, 128
- Wilner, D. J., DePree, C. G., Welch, W. J., & Goss, W. M. 2001, *ApJ*, 550, L81

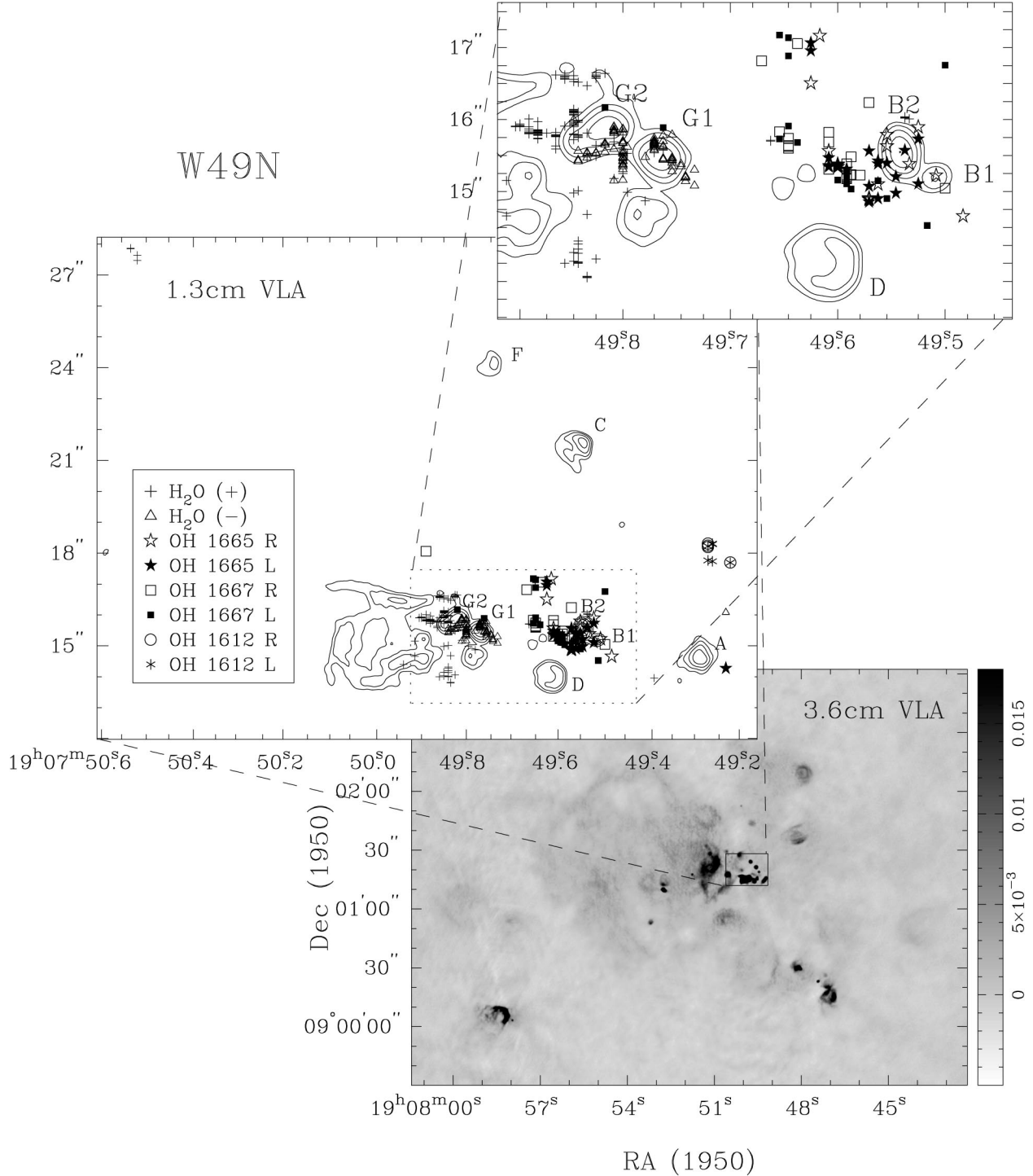


Fig. 1. Overview image of W 49N continuum at 3.6 cm (from Depree et al. (1997)) and 1.3cm insets (from Depree et al. 2000). Beam size for the 3.6cm continuum is $0^{\text{h}}07^{\text{m}}00^{\text{s}}$ $0^{\text{d}}078^{\text{s}}$, PA = -63° . Beam size for the 1.3cm continuum is $0^{\text{h}}02^{\text{m}}00^{\text{s}}$ $0^{\text{d}}024^{\text{s}}$, PA = 8° . Contours are at 10, 20, 40, 80, and $160 \text{ m Jy beam}^{-1}$. H_2O masers (this work) and OH masers (from Argon et al. 2000) are overplotted on the 1.3cm continuum. H_2O masers with positive (negative) velocities with respect to the LSR are represented by crosses (triangles), while OH masers are denoted in the key by their transition (in MHz) with an R (L) for right (left) circularly polarized masers. Absolute alignment between the H_2O and OH maser positions is limited by the absolute positional accuracy of the OH masers ($0^{\text{d}}3$). The alignment between the H_2O masers and the 1.3 cm continuum has an rms error of $0^{\text{d}}01$ (see text for details).

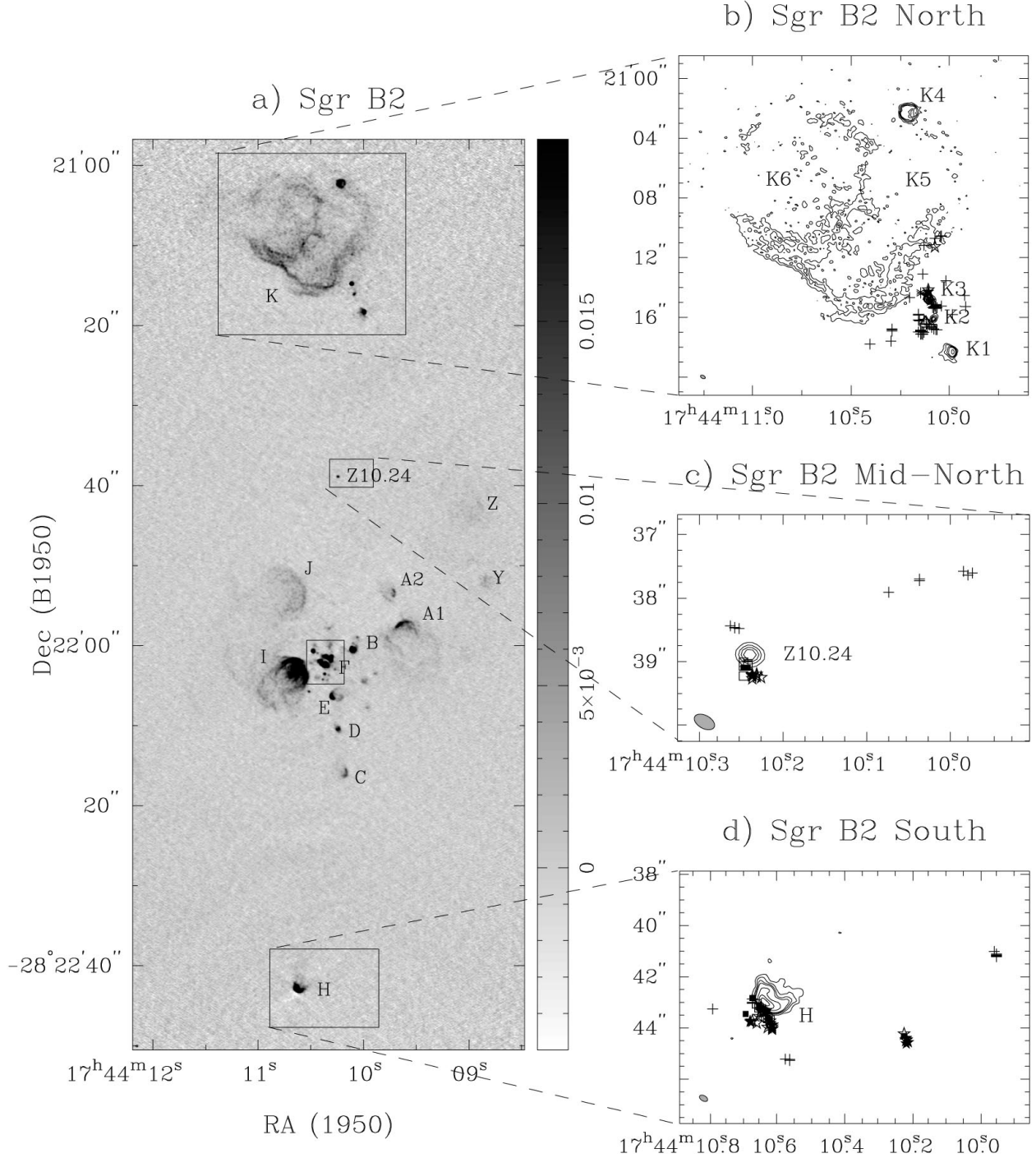


Fig. 2. Overview image of Sgr B2 continuum at 1.3 cm (from Gaume et al. 1995). Beam size is $0\farcs35 \times 0\farcs21$, PA = 61° . Contours for images (b) through (d) are $-2.5, 2.5, 5, 7.5, 10, 20, 30, 40, 50, 60, 70, 80$, and 90% the peak value of 208 mJy. The boxed region around source F is shown in greater detail in Fig. 3. Symbols for masers plotted in gs. (b) – (d) are similar to those plotted in Fig. 1, with crosses for H₂O masers, open (filled) stars for right (left) circular polarized 1665 MHz OH masers, open (filled) boxes for right (left) circular polarized 1667 MHz OH masers, and circles (asterisks) for right (left) circular polarized 1612 MHz OH masers. The alignment error between the H₂O and OH masers is $0\farcs3$, while the alignment error between the H₂O masers and the 1.3 cm continuum is $0\farcs01$.

Sgr B2 Main

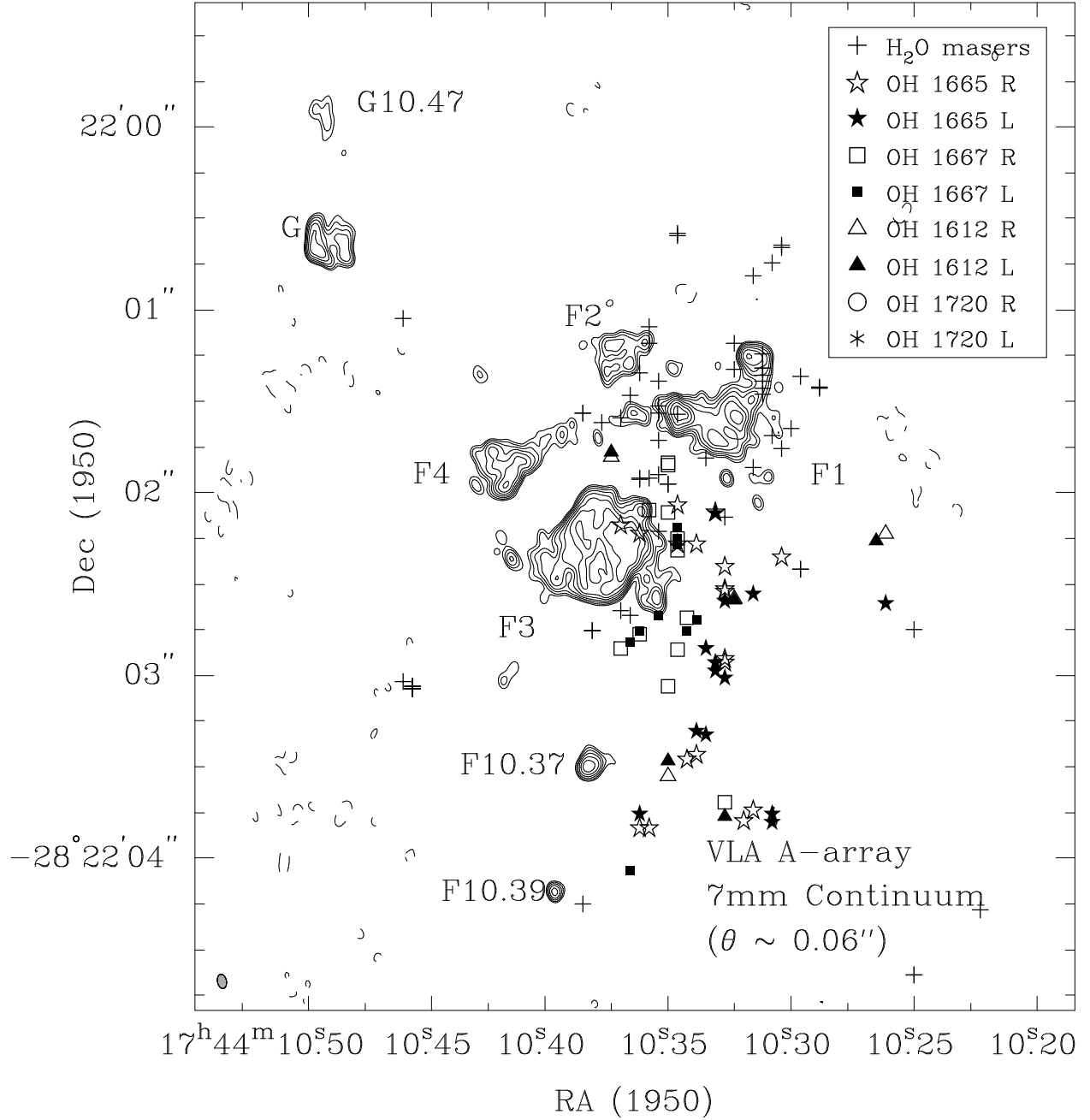


Fig. 3.| Sgr B2 Main. H₂O maser positions (this work) and OH maser positions (Argon et al. 2000) compared to the high resolution 7 mm continuum image of DePree et al., 1998 (beam size = 0.⁰049 – 0.⁰079, PA = 11°). First contour is at the 5 (2.4 mJy beam⁻¹) level. Successive positive contours are at 1.4, 2, 2.8, 4, 5.6, 8, 11.2, and 16 times the first contour. The alignment error between the H₂O and OH masers is 0.⁰3, while the alignment error between the H₂O masers and the 7 mm continuum is 0.⁰05.

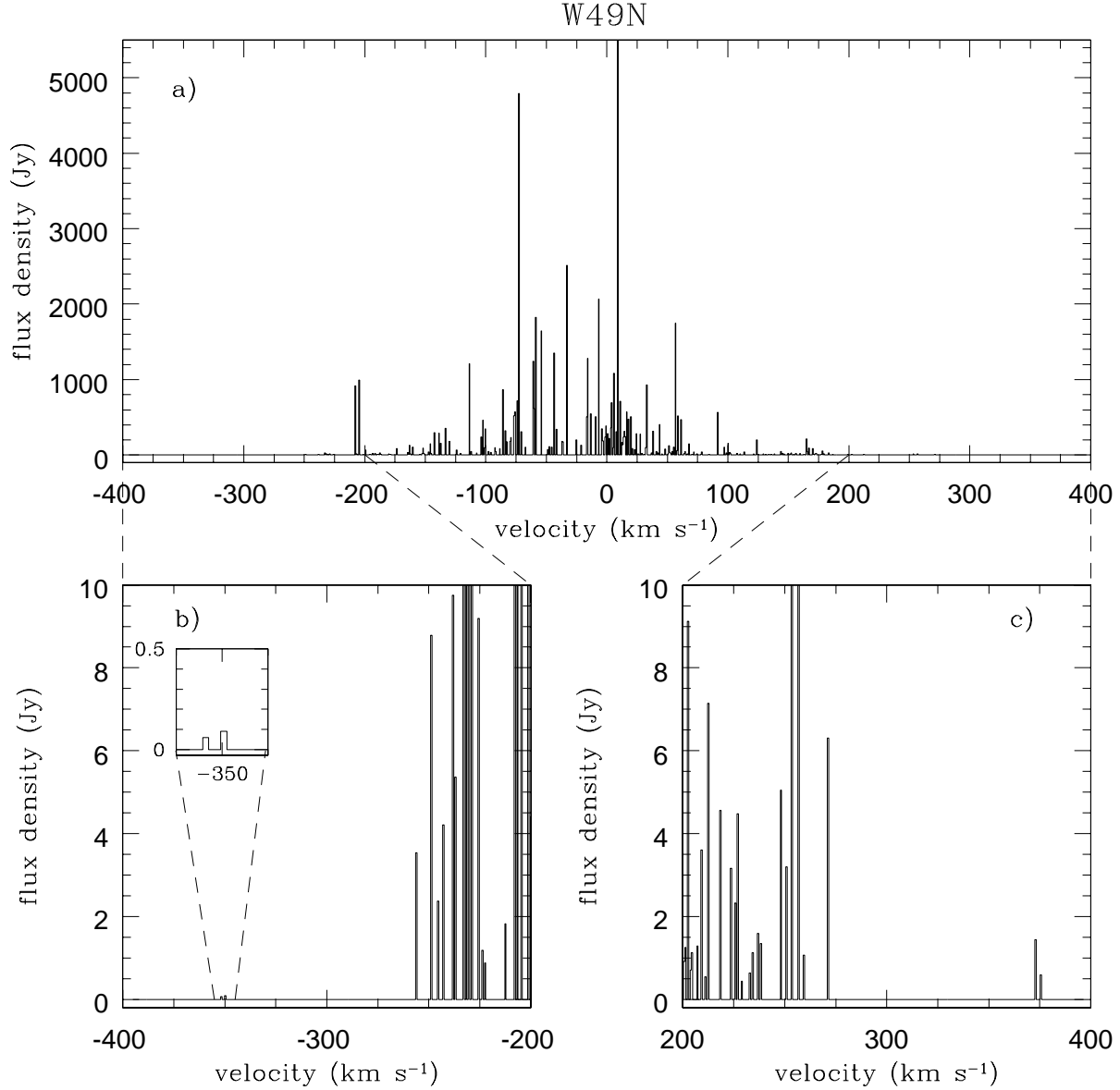


Fig. 4. Spectra of H_2O masers in W 49N observed between 1998 July and 1999 Nov. Velocity is with respect to the LSR. The flux density range has been chosen so that details of the fainter, high velocity features are apparent. The brightest masers are $> 5000 \text{ Jy beam}^{-1}$. See Tab. 2 for a complete list of positions, velocities, and flux densities for these masers.

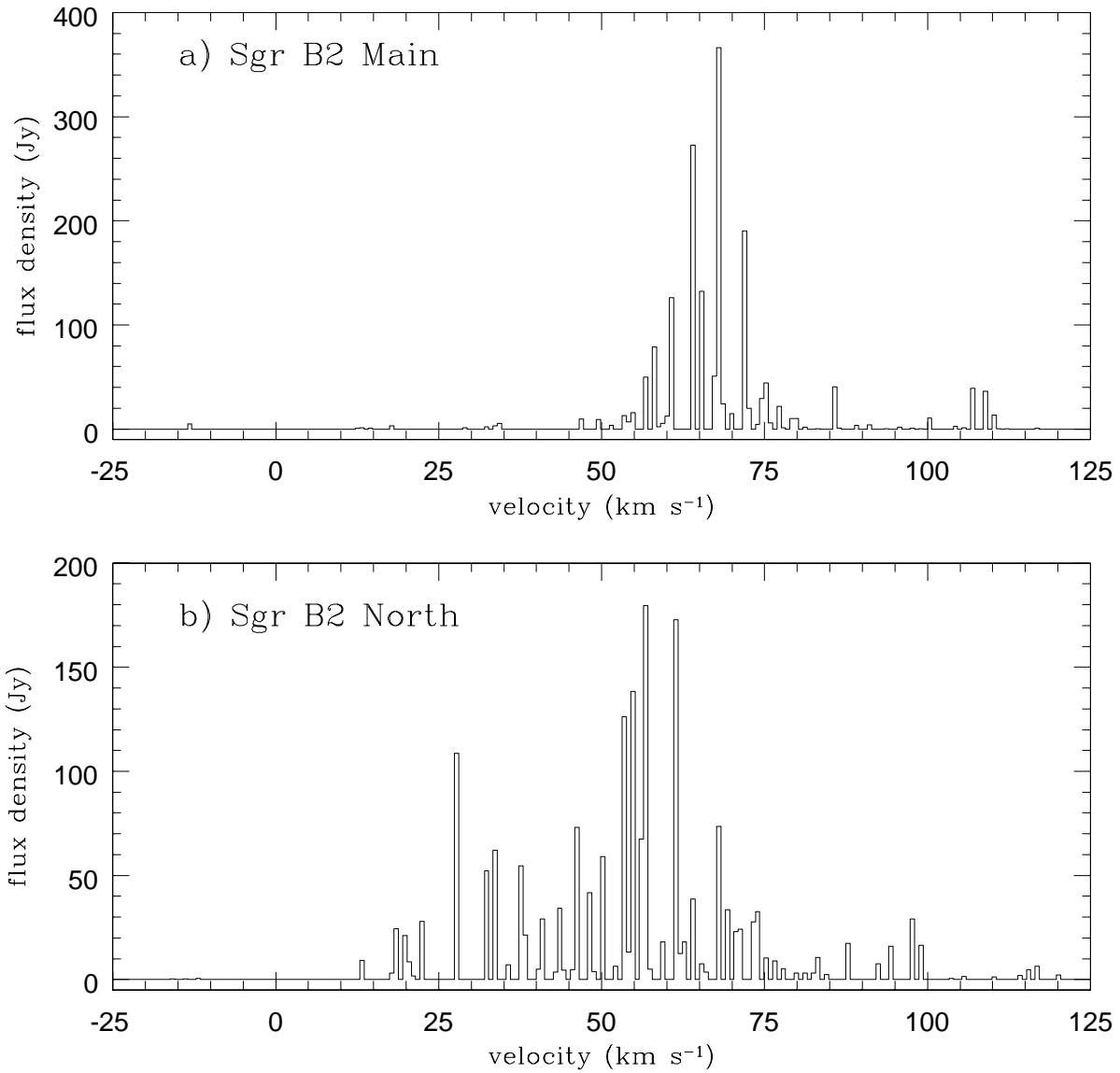


Fig. 5.| Spectra of H_2O masers in Sgr B2 Main (a) and Sgr B2 North (b) observed during 1998 June. See Tables 3 and 4 for a complete list of positions, velocities, and flux densities for these masers.

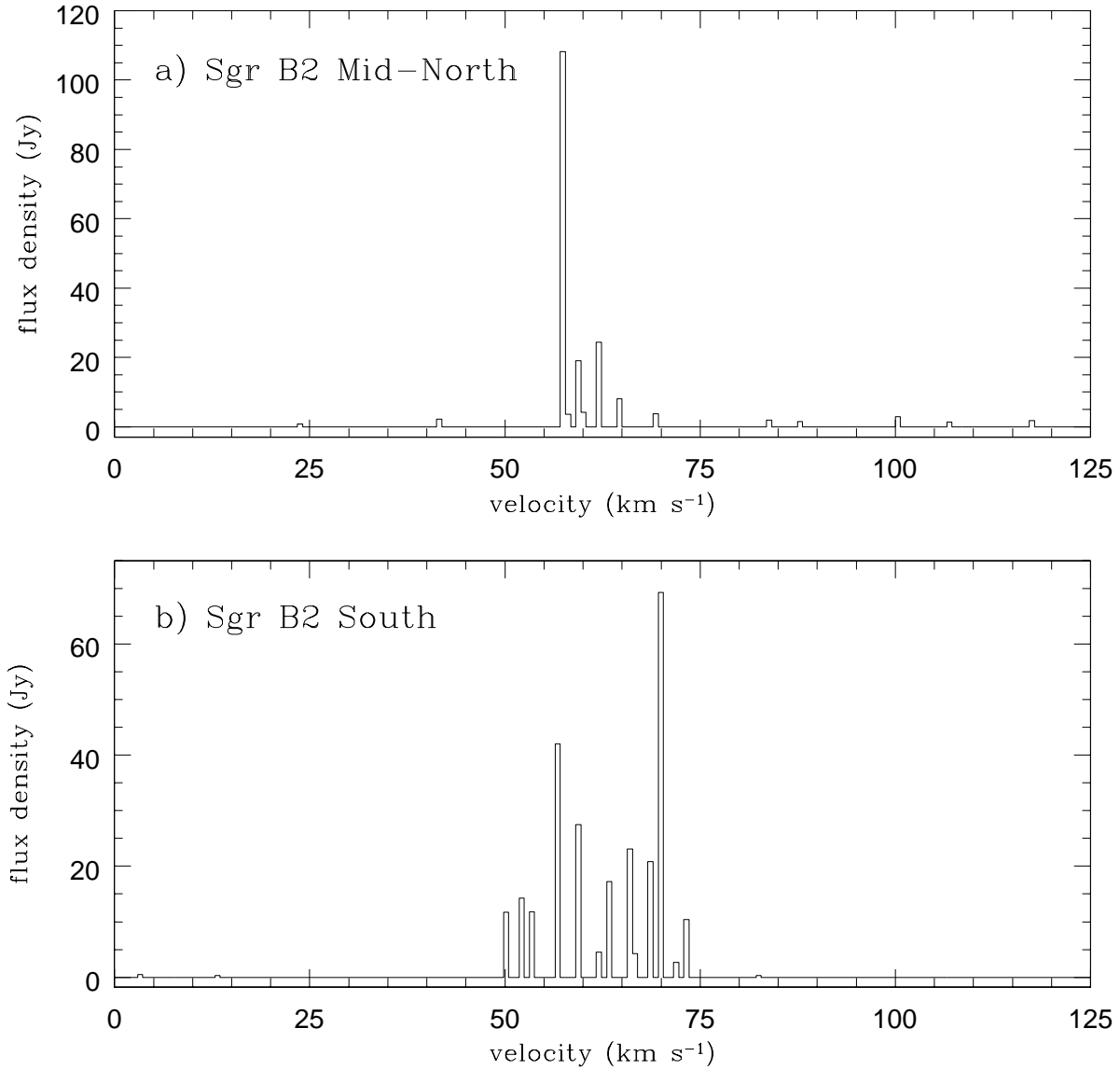


Fig. 6.| Spectra of H₂O masers in Sgr B2 Mid-North (a) and Sgr B2 South (b) observed during 1998 June. See Tables 5 and 6 for a complete list of positions, velocities, and flux densities for these masers.

Table 1. Observational Parameters for VLA 13 mm Observations of W 49N and Sgr B2

Observation Date	VLA Config.	IF 1 Central Vel. (km s ⁻¹)	IF 2 Central Vel. (km s ⁻¹)	beam (arcsec)	P A. (deg)
W 49N					
1998 Jul 24	B	-60, -30, 0, 30, 60	170	0.30	0.27
1998 Aug 24	B	500	170	0.28	0.24
1998 Sep 6	B	-150, -120, -90, 90, 120, 150	170	0.32	0.29
1999 Jun 26	A	-240, -210, -180, 180, 210, 240	170	0.10	0.09
1999 Jul 18	A	-330, -300, -270, 270, 300, 330	170	0.11	0.09
1999 Nov 17	B	-420, -390, -360, 360, 390, 420	170	0.41	0.28
Sgr B2					
1998 Jun 6	BnA	-20, 10, 40, 70, 100	170	0.38	0.18

Table 2. Water Maser Positions and Velocities in W 49A North

(^s) 19 ^h 07 ^m (B 1950)	(^o) 09°01 ⁰ (B 1950)	v _{LSR} (km s ⁻¹)	Flux Density (Jy)	Error (Jy)
49.904	15.91	375.5	0.59	0.20
49.904	15.90	372.8	1.44	0.20
49.898	15.92	271.3	6.30	0.10
49.892	16.01	259.1	1.07	0.03
49.893	15.84	256.5	17.09	0.04
49.894	15.87	253.2	17.39	0.04
49.893	15.84	250.5	3.20	0.02
49.897	15.90	247.9	5.05	0.02
49.889	15.81	238.0	1.34	0.02
49.897	15.90	236.7	1.59	0.02
49.897	15.91	234.1	1.12	0.02
49.882	15.86	232.7	0.64	0.02
49.900	15.94	229.1	0.44	0.03
49.890	15.82	227.1	2.30	0.03
49.882	15.86	226.8	2.18	0.02
49.869	15.59	225.8	2.32	0.03
49.849	16.10	223.8	3.16	0.03
49.850	16.10	218.6	4.56	0.03
49.850	16.10	212.6	7.14	0.03
49.848	15.72	211.3	0.54	0.02
49.887	15.80	209.3	3.61	0.03
49.887	15.90	207.4	1.29	0.03
49.844	15.75	204.7	1.12	0.03
49.887	15.82	204.1	0.71	0.03
49.852	16.14	202.7	9.12	0.03
49.867	15.77	201.4	1.25	0.03
49.844	15.75	200.8	0.91	0.03
49.846	16.10	199.1	9.56	0.04
49.887	15.82	198.1	1.04	0.03
49.867	15.77	197.8	1.55	0.03

Table 2 | Continued

(^s 19 ^h 07 ^m (B 1950))	(⁰ 09°01 ⁰ (B 1950))	v _{LSR} (km s ⁻¹)	Flux Density (Jy)	Error (Jy)
49.887	15.82	196.2	1.73	0.03
49.868	15.79	194.5	6.28	0.03
49.844	15.75	193.2	4.13	0.03
49.853	16.13	191.2	1.35	0.03
49.868	15.79	189.9	2.24	0.02
49.867	15.78	187.3	1.20	0.03
49.844	15.75	186.6	11.01	0.03
49.852	15.79	183.3	22.98	0.05
49.888	15.82	183.3	5.87	0.05
49.844	15.75	181.3	3.68	0.03
49.841	15.99	180.7	2.16	0.03
49.852	16.13	179.3	16.46	0.04
49.866	15.76	178.0	22.12	0.08
49.849	16.09	178.0	21.81	0.08
49.845	15.75	178.0	5.58	0.08
49.841	15.99	178.0	2.45	0.08
49.851	15.80	177.4	10.17	0.05
49.884	15.80	175.4	2.79	0.03
49.879	15.97	174.7	1.55	0.03
49.852	16.11	172.8	5.79	0.04
49.840	15.96	172.8	13.21	0.04
49.879	15.97	172.1	5.58	0.04
49.852	16.12	172.1	5.85	0.04
49.884	15.79	172.1	1.18	0.04
49.841	15.98	170.8	9.8	0.1
49.844	15.75	170.1	84.2	0.2
49.855	16.13	170.1	4.0	0.2
49.852	15.79	168.8	4.57	0.04
49.841	15.98	166.8	94.7	0.2
49.854	16.11	165.8	47.1	0.2

Table 2 | Continued

(^s 19 ^h 07 ^m (B 1950))	(⁰ 09°01 ⁰ (B 1950))	v _{LSR} (km s ⁻¹)	Flux Density (Jy)	Error (Jy)
49.844	15.76	165.2	85.5	0.3
49.844	15.75	164.8	127.1	0.2
49.855	16.13	162.9	7.42	0.04
49.865	15.82	159.9	19.0	0.1
49.849	16.06	156.6	25.1	0.1
49.873	15.81	154.6	7.37	0.02
49.845	15.76	152.6	29.70	0.08
49.855	16.13	152.0	14.98	0.05
49.835	13.80	150.0	21.24	0.06
49.846	15.76	146.7	17.50	0.05
49.846	15.76	145.4	19.92	0.06
49.871	15.78	144.1	8.2	0.1
49.835	13.80	144.1	38.1	0.1
49.850	16.07	138.8	13.29	0.04
49.834	13.80	138.4	2.3	0.1
49.881	15.86	136.2	6.62	0.04
49.900	15.91	133.8	7.45	0.03
49.835	13.80	131.2	9.82	0.04
49.881	15.82	129.2	14.16	0.04
49.844	14.20	127.2	4.54	0.02
49.834	13.81	125.3	9.9	0.2
49.883	15.80	124.0	198.0	0.5
50.538	27.85	121.3	1.42	0.05
49.844	15.79	121.3	12.63	0.05
49.835	13.81	116.7	4.09	0.02
49.843	14.14	116.7	1.53	0.02
49.845	15.78	113.4	42.6	0.1
49.533	16.01	113.4	1.6	0.1
49.846	15.78	110.1	13.67	0.04
50.537	27.85	108.8	0.43	0.03

Table 2 | Continued

(^s 19 ^h 07 ^m (B 1950))	(⁰ 09°01 ⁰ (B 1950))	v _{LSR} (km s ⁻¹)	Flux Density (Jy)	Error (Jy)
49.536	16.02	107.5	20.42	0.07
49.783	14.87	105.2	4.94	0.04
49.837	15.81	102.5	22.5	0.2
49.537	16.02	101.9	35.0	0.2
49.883	15.74	100.5	154.8	0.5
49.836	15.81	99.2	27.6	0.1
49.536	16.03	97.2	102.0	0.2
49.840	15.01	94.6	2.59	0.09
49.666	15.70	93.3	2.14	0.08
49.883	15.74	92.0	565.1	1.5
49.667	15.71	89.3	1.68	0.03
49.844	14.31	87.4	1.17	0.03
49.843	16.52	85.4	2.87	0.04
49.537	16.03	84.7	9.92	0.05
49.803	15.44	83.4	5.38	0.04
49.840	14.01	81.4	2.21	0.06
49.842	14.27	80.1	1.88	0.04
49.814	15.69	78.8	42.4	0.1
49.849	16.61	78.1	6.77	0.08
49.820	15.67	74.8	15.16	0.08
49.856	15.91	72.2	42.3	0.3
49.857	16.59	70.5	5.4	0.1
49.830	16.60	70.5	5.4	0.1
49.882	15.83	67.9	151.2	0.8
49.842	14.02	66.6	17.1	0.2
49.858	16.57	64.6	31.7	0.4
49.824	15.65	64.6	14.4	0.4
49.830	16.59	64.0	20.4	0.4
49.883	15.78	61.3	415.1	2.0
49.833	15.48	61.3	24.4	2.0

Table 2 | Continued

(^s 19 ^h 07 ^m (B 1950))	(⁰ 09°01 ⁰ (B 1950))	v _{LSR} (km s ⁻¹)	Flux Density (Jy)	Error (Jy)
49.840	14.14	61.3	29.7	2.0
49.852	15.93	58.7	520.8	3.4
49.914	14.66	58.0	31.9	2.8
49.829	16.65	58.0	28.6	2.8
49.936	14.40	56.7	148	10
49.880	15.73	56.7	1410	10
49.864	16.62	56.7	90.9	10.0
49.832	14.06	56.7	96.5	10.0
49.851	15.93	55.4	72.8	1.6
49.849	14.98	55.4	35.3	1.6
49.829	16.57	54.1	48.4	0.8
49.834	16.47	52.8	24.2	0.4
49.850	15.95	52.1	35.4	0.5
49.854	16.56	51.4	34.2	0.9
49.836	15.53	51.4	91.0	0.9
49.807	15.53	50.8	20.7	0.7
49.860	16.60	48.1	17.4	0.8
49.837	16.47	48.1	62.8	0.8
49.538	16.04	45.5	12.7	0.4
49.825	15.64	43.8	36.8	0.6
49.882	15.83	43.5	368	10
49.858	16.57	42.5	27.9	0.5
49.841	14.02	41.2	48.0	0.4
49.883	15.81	38.6	319.0	1.5
49.857	16.57	37.2	28.5	0.6
49.865	15.63	33.3	164.3	2.9
49.882	15.83	33.3	767.2	2.9
49.806	15.49	32.6	40.9	2.6
49.857	16.62	32.6	60.0	2.6
49.537	16.04	31.3	11.6	0.7

Table 2 | Continued

(^s 19 ^h 07 ^m (B 1950))	(⁰ 09°01 ⁰ (B 1950))	v _{LSR} (km s ⁻¹)	Flux Density (Jy)	Error (Jy)
49.823	16.64	29.3	12.3	0.8
49.799	15.53	29.3	8.87	0.80
49.538	16.04	27.4	31.3	1.1
49.883	15.85	27.4	245.9	1.1
49.825	16.62	26.0	13.4	0.6
49.537	16.03	24.7	26.3	0.8
49.847	14.00	24.1	40.0	1.0
49.882	15.85	24.1	218.8	1.0
49.795	14.99	23.4	45.7	0.9
50.536	27.87	23.4	24.5	0.9
50.536	27.85	21.4	39.4	1.4
49.775	15.59	20.8	18.9	1.8
49.807	15.52	20.8	27.2	1.8
49.883	15.84	20.1	243.1	2.3
49.853	16.53	19.5	239.1	2.8
49.912	15.15	19.5	27.1	2.8
49.849	14.03	18.1	478	11
49.849	15.92	16.2	285.5	3.8
49.810	15.82	16.2	284.5	3.8
49.770	15.54	15.5	85.1	2.9
49.387	13.96	15.5	73.8	2.9
49.825	15.49	14.9	89.3	4.1
49.885	15.85	14.5	314.0	1.8
50.522	27.64	13.8	237.3	3.0
49.856	16.56	13.2	36.4	2.8
49.853	14.15	13.2	103.6	2.8
49.855	15.92	12.5	102.8	4.2
49.837	13.82	12.5	69.4	4.2
49.886	15.85	11.2	424.0	7.9
49.768	15.60	11.2	290.3	7.9

Table 2 | Continued

(^s 19 ^h 07 ^m (B 1950))	(⁰ 09°01 ⁰ (B 1950))	v _{LSR} (km s ⁻¹)	Flux Density (Jy)	Error (Jy)
49.803	15.59	9.2	5040	30
49.838	14.68	9.2	481	31
49.857	14.00	7.9	313	24
49.808	15.25	5.9	1080	10
50.522	27.47	5.3	98.8	5.0
49.853	15.90	3.9	384.0	3.1
49.768	15.57	3.9	306.8	3.1
49.801	15.83	3.3	362.2	2.1
49.853	15.99	2.0	220.8	1.6
49.814	15.18	0.7	282.0	1.4
49.854	16.00	-0.7	109.6	1.8
49.840	15.44	-0.7	161.1	1.8
49.769	15.63	-0.7	118.0	1.8
49.814	15.15	-1.3	242.5	1.7
49.842	15.42	-3.3	188.2	2.1
49.748	15.38	-3.9	349.9	2.6
49.804	15.57	-6.6	2070	10
49.771	15.70	-9.2	510.4	3.1
49.771	15.69	-13.2	544.2	2.8
49.771	15.62	-15.8	909	22
49.804	15.16	-15.8	373	22
49.803	15.31	-16.8	506.5	3.3
49.809	15.83	-21.4	133.4	1.2
49.772	15.66	-25.4	126.5	1.0
49.811	15.86	-25.4	77.8	1.0
49.804	15.35	-33.3	2520	10
49.771	15.64	-36.6	178.4	1.7
49.810	15.81	-37.2	182.4	1.4
49.771	15.69	-41.8	339.3	3.7
49.802	15.68	-43.8	1350	10

Table 2 | Continued

(^s 19 ^h 07 ^m (B 1950))	(⁰ 09°01 ⁰ (B 1950))	v _{LSR} (km s ⁻¹)	Flux Density (Jy)	Error (Jy)
49.773	15.59	-45.8	107.7	9.8
49.814	15.90	-47.5	109.6	0.6
49.805	15.37	-48.8	71.6	0.5
49.803	15.67	-54.1	1650	10
49.771	15.69	-58.7	1830	10
49.803	15.68	-60.0	619.3	4.0
49.771	15.69	-60.7	1240	10
49.802	15.68	-67.2	106.3	1.1
49.833	15.53	-70.9	308.7	3.4
49.772	15.68	-72.5	4791	2
49.833	15.53	-73.8	716.2	4.5
49.802	15.68	-76.2	570.6	1.7
49.771	15.57	-76.8	523.5	1.7
49.832	15.53	-79.5	233.6	0.9
49.812	15.89	-80.1	178.9	0.9
49.805	15.42	-82.8	177.6	0.8
49.832	15.53	-84.1	325.2	0.7
49.832	15.53	-86.1	868.9	1.8
49.767	15.62	-88.7	88.9	0.3
49.799	15.62	-92.0	45.8	0.2
49.770	15.64	-92.6	98.7	0.2
49.831	15.54	-95.9	32.8	0.2
49.805	15.53	-97.9	48.3	0.2
49.772	15.67	-100.5	349.8	0.8
49.833	15.54	-100.9	99.8	0.8
49.775	15.74	-102.5	461.7	0.9
49.773	15.71	-103.6	197.4	0.8
49.832	15.54	-103.8	40.2	0.3
49.807	15.53	-107.5	28.1	0.5
49.805	15.31	-112.1	44.7	1.3

Table 2 | Continued

(^s 19 ^h 07 ^m (B 1950))	(⁰ 09°01 ⁰ (B 1950))	v _{LSR} (km s ⁻¹)	Flux Density (Jy)	Error (Jy)
49.771	15.67	-113.4	1210	3
49.841	15.56	-120.7	19.0	0.5
49.805	15.86	-123.9	67.8	0.6
49.805	15.46	-129.9	182.4	0.5
49.807	15.54	-133.2	59.6	0.3
49.805	15.43	-133.6	77.8	0.7
49.772	15.67	-133.6	219.0	0.7
49.803	15.70	-137.5	159.2	0.9
49.772	15.66	-138.8	289.1	0.7
49.771	15.67	-142.8	299.6	0.7
49.801	15.87	-145.4	22.0	0.3
49.771	15.67	-146.1	152.6	0.4
49.819	15.65	-147.4	31.6	0.2
49.839	15.47	-147.4	11.5	0.2
49.817	15.67	-151.3	22.2	0.1
49.771	15.66	-152.0	90.1	0.2
49.802	15.82	-152.6	19.8	0.2
49.819	15.65	-154.6	6.71	0.07
49.772	15.65	-160.3	103.8	0.2
49.805	15.42	-162.5	13.94	0.05
49.772	15.65	-162.9	130.8	0.2
49.767	15.45	-163.6	9.8	0.3
49.804	15.46	-164.2	33.7	0.1
49.805	15.87	-165.5	1.30	0.07
49.810	15.59	-166.2	1.36	0.08
49.756	15.35	-168.8	2.34	0.04
49.767	15.45	-169.5	3.39	0.04
49.772	15.66	-173.4	84.7	0.2
49.767	15.45	-174.7	2.60	0.04
49.744	15.14	-174.7	1.79	0.04

Table 2 | Continued

(^s 19 ^h 07 ^m (B 1950))	(⁰ 09°01 ⁰ (B 1950))	v _{LSR} (km s ⁻¹)	Flux Density (Jy)	Error (Jy)
49.815	15.84	-174.7	1.04	0.04
49.747	15.35	-175.4	1.59	0.03
49.815	15.83	-178.7	4.61	0.05
49.764	15.70	-178.7	2.44	0.05
49.784	15.48	-179.3	4.92	0.05
49.762	15.78	-179.3	2.18	0.05
49.805	15.48	-180.0	12.51	0.05
49.747	15.35	-180.7	2.08	0.05
49.765	15.46	-181.3	2.12	0.04
49.747	15.35	-184.6	5.81	0.04
49.761	15.79	-185.3	0.75	0.04
49.747	15.35	-186.6	7.33	0.07
49.763	15.44	-186.6	4.33	0.07
49.756	15.28	-187.2	27.56	0.08
49.771	15.68	-188.5	11.18	0.06
49.763	15.44	-189.2	8.81	0.06
49.754	15.47	-189.9	4.60	0.06
49.747	15.35	-191.2	22.18	0.06
49.747	15.35	-193.6	21.96	0.06
49.764	15.45	-194.9	5.50	0.06
49.770	15.68	-195.5	12.16	0.07
49.754	15.47	-195.8	3.56	0.11
49.754	15.46	-196.2	2.89	0.07
49.804	15.48	-199.5	67.6	0.1
49.747	15.35	-200.1	4.41	0.10
49.808	15.38	-201.5	10.69	0.07
49.804	15.48	-204.7	991.1	1.9
49.747	15.35	-206.7	13.30	0.29
49.803	15.48	-208.0	917.2	1.9
49.763	15.45	-212.6	1.82	0.03

Table 2 | Continued

(^s) 19 ^h 07 ^m (B1950)	(⁰) 09°01 ⁰ (B1950)	v _{LSR} (km s ⁻¹)	Flux Density (Jy)	Error (Jy)
49.742	15.19	-222.3	0.88	0.03
49.734	15.30	-223.6	1.18	0.03
49.818	15.55	-225.5	0.64	0.03
49.804	15.48	-225.5	8.55	0.03
49.759	15.44	-228.8	15.55	0.04
49.742	15.20	-230.1	10.67	0.09
49.805	15.48	-231.5	15.89	0.05
49.759	15.43	-232.8	28.46	0.09
49.742	15.21	-236.7	5.36	0.03
49.759	15.43	-238.0	9.75	0.03
49.754	15.40	-242.6	4.21	0.02
49.759	15.43	-245.3	2.37	0.02
49.734	15.08	-248.5	8.79	0.03
49.734	15.08	-255.8	3.54	0.03
49.231	16.09	-349.5	0.09	0.01
49.234	16.08	-352.1	0.06	0.01

Note. | Relative positional errors are 0.005 arcseconds and . Absolute errors are 0.05.

Table 3. Water Maser Positions and Velocities in SgrB2 Main

(^s) 17 ^h 44 ^m (B 1950)	(⁰) -28°22 ⁰ (B 1950)	v _{LSR} (km s ⁻¹)	Flux Density (Jy)	Error (Jy)
10.361	01.92	117.1	0.67	0.02
10.290	01.43	111.9	0.44	0.01
10.362	01.92	111.2	0.47	0.01
10.296	02.42	109.9	13.46	0.03
10.457	03.07	109.2	36.60	0.05
10.457	03.07	107.2	2.39	0.03
10.296	02.42	106.6	36.74	0.04
10.223	04.28	105.9	0.44	0.02
10.362	01.93	105.9	0.93	0.02
09.800	05.74	104.6	1.32	0.02
10.456	03.07	104.0	1.17	0.02
10.457	03.07	100.0	10.81	0.03
09.802	05.73	99.3	0.54	0.03
10.457	03.06	97.4	0.77	0.04
10.353	01.95	95.4	1.81	0.02
10.250	04.64	93.4	0.52	0.02
10.313	01.32	90.8	4.32	0.02
10.352	01.95	88.8	1.64	0.02
10.386	01.56	88.8	1.26	0.02
10.250	04.64	88.8	0.96	0.02
10.314	01.32	86.2	0.95	0.03
10.385	01.56	85.5	40.63	0.04
10.354	01.71	82.9	0.56	0.02
10.315	00.81	81.2	1.88	0.02
10.382	02.76	79.9	10.07	0.03
10.354	01.90	79.2	10.06	0.03
10.460	03.03	77.9	1.45	0.04
10.347	01.57	77.2	5.60	0.04
10.382	02.76	77.2	16.16	0.04
10.346	00.59	75.9	6.12	0.07

Table 3 | Continued

(s) 17 ^h 44 ^m (B1950)	(°) -28°22 ⁰ (B1950)	v _{LSR} (km s ⁻¹)	Flux Density (Jy)	Error (Jy)
10.382	02.76	75.3	36.47	0.08
10.295	01.37	75.3	7.81	0.08
10.336	01.81	74.6	29.41	0.06
10.360	01.18	74.0	4.44	0.06
10.388	04.25	72.6	19.85	0.08
10.457	03.06	72.0	8.3	0.2
10.324	01.33	72.0	31.9	0.2
10.303	01.76	72.0	7.1	0.2
10.371	01.59	72.0	143.0	0.2
10.290	01.42	70.0	14.6	0.4
10.458	03.06	68.7	10.6	0.2
10.310	01.69	68.7	13.8	0.2
10.377	01.62	68.0	366.1	0.4
10.312	01.39	67.4	50.9	0.3
10.301	01.65	65.4	132.4	0.2
10.313	01.46	64.1	272.7	0.3
10.314	01.36	60.8	126.3	0.3
10.360	01.09	60.1	12.4	0.1
10.315	01.86	59.5	5.35	0.10
10.348	00.58	58.8	2.11	0.09
10.313	01.43	58.1	78.8	0.1
10.327	02.13	56.8	2.7	0.2
10.363	01.34	56.5	47.4	0.3
10.303	00.65	54.5	15.8	0.2
10.355	01.56	53.8	7.1	0.2
10.303	00.66	53.2	13.1	0.2
10.356	01.52	51.2	3.45	0.13
10.462	01.05	49.2	9.26	0.10
10.357	01.39	46.6	9.65	0.12
10.354	02.21	34.1	5.64	0.08

Table 3 | Continued

(^s) 17 ^h 44 ^m (B 1950)	(⁰) -28°22 ⁰ (B 1950)	v _{LSR} (km s ⁻¹)	F lux D ensity (Jy)	E rr or (Jy)
10.249	02.75	33.4	3.33	0.10
10.312	01.24	32.1	2.40	0.08
10.323	01.18	29.1	1.41	0.12
10.369	02.67	17.9	3.38	0.33
10.308	00.74	14.6	0.90	0.02
10.371	02.65	13.3	1.47	0.03
10.366	01.47	12.6	0.83	0.02
09.758	00.64	-13.4	4.95	0.02

Note. | Relative positional errors are 0.005 in and . Absolute errors are 0.05.

Table 4. Water Maser Positions and Velocities in SgrB2 North

(^s 17 ^h 44 ^m (B1950))	(⁰ -28°21 ⁰ (B1950))	v _{LSR} (km s ⁻¹)	Flux Density (Jy)	Error (Jy)
10.044	15.24	119.8	2.19	0.03
10.064	16.83	116.5	6.51	0.04
09.924	14.54	115.8	4.85	0.04
10.071	15.21	114.5	2.05	0.02
10.087	15.34	110.5	1.27	0.03
10.162	15.84	105.3	1.60	0.03
10.089	16.67	103.3	0.63	0.02
10.089	16.68	99.3	16.37	0.07
10.089	16.68	98.0	19.91	0.08
10.161	15.85	97.4	9.14	0.08
10.083	15.30	94.7	6.14	0.04
10.073	15.24	94.1	9.91	0.05
10.089	16.68	92.1	7.57	0.04
10.067	15.20	87.5	17.51	0.07
10.069	15.18	84.5	1.81	0.03
10.118	16.45	84.2	0.54	0.03
10.155	16.99	83.2	8.37	0.05
10.082	15.39	83.2	2.25	0.05
10.071	15.14	82.5	3.09	0.04
09.984	15.81	81.2	3.07	0.03
09.917	15.28	79.9	3.22	0.04
10.070	15.22	77.9	5.28	0.05
10.116	16.44	76.6	3.56	0.07
10.092	16.46	76.6	5.43	0.07
10.131	11.18	75.3	1.98	0.10
10.039	10.54	75.3	8.40	0.10
10.067	15.19	74.0	3.13	0.11
10.131	17.01	74.0	17.0	0.1
10.039	10.56	74.0	12.4	0.1
10.405	17.79	73.3	27.6	0.1

Table 4 | Continued

(s) 17 ^h 44 ^m (B1950)	(°) -28°21 ⁰ (B1950)	v _{LSR} (km s ⁻¹)	Flux Density (Jy)	Error (Jy)
10.294	16.82	71.3	24.3	0.2
10.405	17.79	70.7	23.0	0.2
10.146	16.95	69.3	33.5	0.4
10.293	16.82	68.0	73.6	0.5
10.135	13.10	66.0	3.6	0.3
10.296	17.60	65.4	3.3	0.3
09.467	12.36	65.4	4.4	0.3
10.017	13.55	64.1	38.7	0.3
10.293	16.83	62.8	18.1	0.3
10.143	16.94	62.1	12.5	0.4
10.065	15.31	61.4	172.9	0.7
10.293	16.79	59.5	2.2	0.1
10.140	16.94	59.5	16.0	0.1
10.063	15.36	57.1	5.1	0.4
10.150	16.86	56.5	160.2	0.6
10.074	10.70	56.5	19.2	0.6
10.203	14.67	55.8	67.5	0.5
10.146	16.90	55.1	131.9	0.5
10.155	15.80	54.5	6.5	0.4
10.157	16.19	53.8	7.1	0.3
10.292	16.92	53.8	6.0	0.3
10.140	16.97	53.2	126.2	0.5
10.151	16.24	51.9	6.5	0.3
10.068	15.40	49.9	59.1	0.3
10.161	15.83	48.6	3.9	0.2
10.140	16.97	47.9	41.7	0.2
10.068	15.40	45.9	73.2	0.3
10.158	16.18	45.3	4.7	0.1
10.114	16.66	44.0	4.6	0.1
10.138	16.98	43.3	34.2	0.1

Table 4 | Continued

(^s) 17 ^h 44 ^m (B 1950)	(⁰) -28°21 ⁰ (B 1950)	v _{LSR} (km s ⁻¹)	Flux Density (Jy)	Error (Jy)
10.093	16.63	42.6	3.54	0.08
10.139	16.98	40.7	29.1	0.1
10.114	16.65	40.0	5.10	0.08
10.092	16.62	38.0	21.5	0.1
10.136	17.11	37.4	54.5	0.2
10.072	16.83	35.4	7.19	0.10
10.137	17.15	33.4	62.2	0.2
10.136	17.15	32.1	52.2	0.2
10.142	17.12	27.8	108.6	0.4
10.143	17.13	22.5	27.9	0.1
10.047	10.57	21.2	1.63	0.05
10.078	16.78	20.5	8.59	0.08
10.143	17.13	19.9	21.16	0.08
10.142	17.11	18.6	24.33	0.08
10.100	16.51	17.9	3.11	0.06
10.134	16.13	13.3	9.14	0.04
10.124	16.28	-12.1	0.49	0.02
10.122	16.29	-14.1	0.42	0.03
10.092	16.57	-16.1	0.38	0.03

Note. | Relative positional errors are 0.005 in and . Absolute errors are 0.05.

Table 5. Water Maser Positions and Velocities in SgrB2 Mid-North

(^s) 17 ^h 44 ^m (B 1950)	(^o) -28°21 ⁰ (B 1950)	v _{LSR} (km s ⁻¹)	Flux Density (Jy)	Error (Jy)
09.972	37.60	117.8	1.81	0.02
09.972	37.60	106.6	1.36	0.04
09.972	37.60	100.0	2.86	0.03
10.259	38.47	88.1	1.55	0.03
10.259	38.46	83.8	1.87	0.03
09.971	37.60	69.3	3.8	0.3
10.263	38.44	64.7	8.1	0.2
10.263	38.44	62.1	24.4	0.3
10.038	37.70	60.1	4.2	0.2
10.074	37.91	59.5	19.0	0.1
10.253	38.48	57.8	3.7	0.2
10.035	37.73	57.5	108.1	0.3
09.977	37.64	41.3	2.22	0.05
09.986	37.58	23.8	0.78	0.04

Note. | Relative positional errors are 0.005 in and . Absolute errors are 0.05.

Table 6. Water Maser Positions and Velocities in SgrB2 South

(^s) 17 ^h 44 ^m (B1950)	(^o) -28°22 ⁰ (B1950)	v _{LSR} (km s ⁻¹)	Flux Density (Jy)	Error (Jy)
09.949	41.20	82.8	0.29	0.02
09.951	41.18	73.3	10.4	0.1
10.671	42.87	72.0	2.7	0.2
10.580	45.22	70.0	69.3	0.3
10.672	43.02	68.7	20.8	0.2
10.793	43.26	66.7	4.3	0.2
10.672	43.01	66.0	20.0	0.2
10.567	45.27	66.0	3.1	0.2
10.673	43.03	63.4	17.2	0.2
10.568	45.23	62.1	4.5	0.2
09.949	41.11	59.5	27.5	0.1
09.953	41.22	56.5	42.0	0.3
09.950	41.17	53.2	11.8	0.3
09.951	41.16	51.9	14.2	0.2
09.951	41.16	49.9	11.7	0.2
09.958	41.01	13.3	0.37	0.03
09.959	41.01	3.4	0.52	0.03

Note. | Relative positional errors are 0.005 in and . Absolute errors are 0.05.